Oxygen Discharge and Post-Discharge Kinetics Experiments and Modeling for the Electric Oxygen−Iodine Laser System†

A. D. Palla,‡ J. W. Zimmerman,§ B. S. Woodard,§ D. L. Carroll,*,‡ J. T. Verdeyen,‡ T. C. Lim,§ and W. C. Solomon§

CU Aerospace, 2100 South Oak Street, Champaign, Illinois 61820, and University of Illinois at Urbana-Champaign, 306 Talbot Lab, 104 South Wright Street, Urbana, Illinois 61801

Received: December 29, 2006; In Final Form: March 15, 2007

Laser oscillation at 1315 nm on the $I(^2P_{1/2}) \rightarrow I(^2P_{3/2})$ transition of atomic iodine has been obtained by a near resonant energy transfer from $O_2(a^1\Delta)$ produced using a low−pressure oxygen/helium/nitric oxide discharge. In the electric discharge oxygen−iodine laser (ElectricOIL) the discharge production of atomic oxygen, ozone, and other excited species adds levels of complexity to the singlet oxygen generator (SOG) kinetics which are not encountered in a classic purely chemical $O_2(a^1\Delta)$ generation system. The advanced model BLAZE-IV has been introduced to study the energy-transfer laser system dynamics and kinetics. Levels of singlet oxygen, oxygen atoms, and ozone are measured experimentally and compared with calculations. The new BLAZE-IV model is in reasonable agreement with O_3, O atom, and gas temperature measurements but is under-predicting the increase in $O_2(a^1\Delta)$ concentration resulting from the presence of NO in the discharge and under-predicting the $O_2(b^1\Sigma)$ concentrations. A key conclusion is that the removal of oxygen atoms by NO_X species leads to a significant increase in $O_2(a^1\Delta)$ concentrations downstream of the discharge in part via a recycling process; however, there are still some important processes related to the NO_X discharge kinetics that are missing from the present modeling. Further, the removal of oxygen atoms dramatically inhibits the production of ozone in the downstream kinetics.

1. Introduction

The classical chemical oxygen−iodine laser first reported by McDermott et al.[1] operates on the electronic transition of the iodine atom at 1315 nm, $I(^2P_{1/2}) \rightarrow I(^2P_{3/2})$ [denoted hereafter as I* and I, respectively]. The lasing state I* is produced by near resonant energy transfer with the singlet oxygen metastable $O_2(a^1\Delta)$ [also denoted hereafter as $O_2(a)$]. Conventionally, a chemical two-phase process is used to produce the $O_2(a)$ at the interface of liquid basic H_2O_2 and Cl_2 gas. Zalesskii[2] and Fournier et al.[3] made early attempts to use electric discharges for $O_2(a)$ production and transfer energy to iodine for lasing, but did not obtain positive gain. Since then, various groups[4−9] have investigated other continuous flowing systems and have measured $O_2(a)$ yields in excess of 15%, a necessary condition for positive gain at room temperature. Carroll et al.[10] achieved positive gain and reported lasing in the same system in subsequent work.[11] One key difference between the traditional chemical excitation route and the electrical one is the presence of atomic oxygen levels on the same order as the $O_2(a)$. Atomic oxygen depletes the upper laser level,[12,13] I*, and must be controlled.[14,15] This was accomplished by the use of NO_2 titration made downstream from the discharge or by adding NO to the discharge flow or downstream of the discharge; all of these approaches resulted in the oxygen atoms being depleted to a level such that there were still enough oxygen atoms to dominate the I_2 dissociation process but low enough such that the power loss through the I* + O quenching channel is not seriously detrimental. Subsequent efforts have demonstrated gain[16−18] and lasing[17,18] in other ElectricOIL configurations since the first demonstrations.[10,11] ElectricOIL discharge models[8,19−22] have been developed, and post-dishcarge kinetics-gain-laser modeling[4,15] has been performed. For an excellent topical review of discharge production of $O_2(a)$ and ElectricOIL studies, see Ionin et al.[8]

In this work, measurements and modeling of singlet oxygen, oxygen atoms, and ozone are reported. The advanced discharge-laser model BLAZE-IV which couples fluid dynamics, chemical kinetics, and plasma dynamics, is compared to established helium discharge data and calculations and applied to model the more complex He/O_2 discharge used in ElectricOIL. Important modeling results are the variation of power deposition into $O_2(a)$ as a function of plasma *E*/*N* (electric-field to gas-density ratio) for increasing $O_2(a)$ yield and calculation of the levels of oxygen atoms and ozone created in the discharge and afterglow, both with and without NO in the discharge flow. Backed by experimental results, the modeling work leads to two important conclusions: (i) NO in the discharge depletes oxygen atoms via a recycling mechanism, thereby reducing associated power-loss mechanisms (e.g., $I^* + O(^3P) \rightarrow I + O(^3P)$], and (ii) ozone formation for the cases of interest in this study is small and is dramatically reduced when small amounts of NO (∼1%) are added to the discharge flow. The BLAZE-IV model provides reasonable agreement with measured levels of singlet oxygen, oxygen atoms, ozone, and gas temperature. However, the $O_2(a)$ data indicates that there still appears to be some important missing discharge kinetics related to NO and/or NO_2, the calculated concentration of $O_2(b)$ is generally lower

† Part of the special issue "M. C. Lin Festschrift".

* Corresponding author. E-mail: carroll@cuaerospace.com. Phone: 1-217-333-8274. Fax: 1-217-244-7757. Web site: http://www.cuaerospace.com.

‡ CU Aerospace.

§ University of Illinois at Urbana-Champaign.

10.1021/jp069003+ CCC: $37.00
Published on Web 04/27/2007

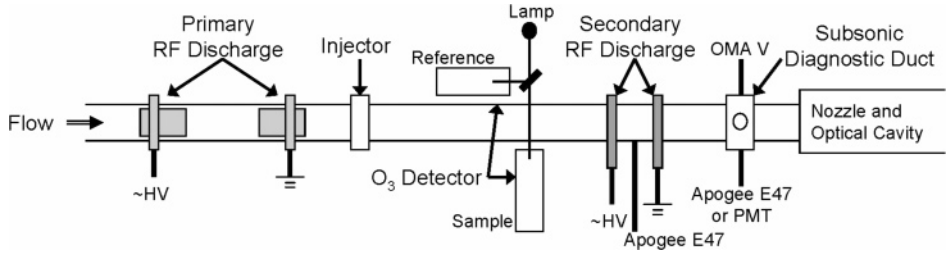

Figure 1. Schematic of typical ElectricOIL diagnostic setup.

than measured, and the calculated concentration of O_3 is generally higher than measured.

2. Experimental Apparatus

A block diagram of the typical setup for diagnostic operations is shown in Figure 1. The subsonic diagnostic duct has four windows through which simultaneous measurements are made of the optical emission from $O_2(a)$ at 1268 nm and $O_2(b^1\Sigma)$ [denoted $O_2(b)$ hereafter] at 762 nm. Optical emission and absorption data are also taken directly through Pyrex and quartz tubes in the flow system, which can be reconfigured for a variety of studies. The primary discharge consists of two hollow cathodes inside a 5 cm diameter quartz tube and has a standard electrode separation of 25.4 cm. For the kinetics studies here, various flow tube and injector configurations were used, and they are discussed as necessary. A Roper Scientific Optical Multi-channel Analyzer (OMA-V) was used for measurements at 1268 nm. An Apogee E47 CCD array coupled to a Roper Scientific/Acton Research 150-mm monochromator was implemented to measure the emission of $O_2(b)$ at 762 nm, as well as the emissions of excited atomic oxygen at 777 nm and excited argon at 750.4 nm. The 777 nm (O*) and 750.4 nm (Ar*) lines are used to perform actinometry with a secondary discharge to monitor oxygen atoms.[23] The broadband emission of NO_2* was measured using a Hamamatsu R955 photomultiplier tube (PMT) with a narrowband 580 nm filter and a 50 mm focal length Pyrex collection lens. The NO_2* emission was then used to monitor oxygen atom decay and titrations. All emission diagnostics were fiber coupled using Oriel model no. 77538 glass fiber bundles. The concentration of ozone formed in the discharge afterglow was measured using the Physical Sciences, Inc., microabsorbance ozone monitor,[24] which operates using ratiometric absorption of a radiation at 254 nm from a mercury lamp and has a detection limit of $\sim 5 \times 10^{11}$ molecules/cm^3.

Micro-Motion CMF and Omega FMA mass flow meters were used to measure the flow rates of the gases. Pressures in the flow tubes were measured by capacitance manometers. Incident and reflected powers to the radio frequency (RF) matching network were measured by a series of Bird Thruline model 43 wattmeters (RF "system power" is the difference of the incident and reflected powers, but typically the reflected power is ≈ 0). The discharge was excited with power provided by an ENI OEM-12A generator at 13.56 MHz through the matching network.

3. Experimental Results

3.1. Increased $O_2(a)$ Concentrations with Nitric Oxide. Discovering an increase in discharge $O_2(a)$ concentrations with the addition of small quantities of nitric oxide (NO) played a vital role in the development of the first electrically excited oxygen−iodine laser.[10,11,14] The path to a higher gain medium required a method of decreasing oxygen atom concentration to control the rapid loss of $O_2(a)$ observed with iodine addition.

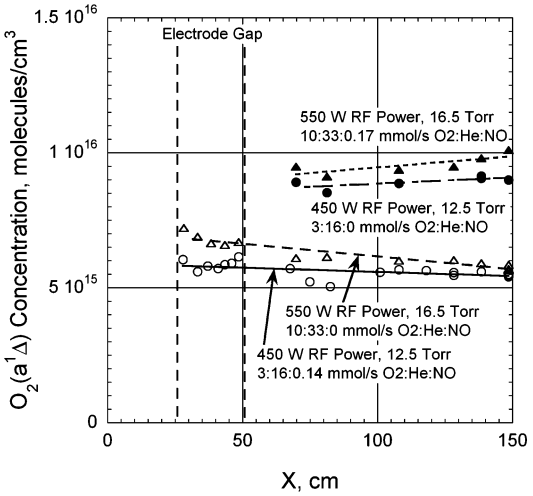

Figure 2. Effect on NO addition on $O_2(a)$ concentration as a function of position and flow conditions. The electrode gap is the region between the hollow cathode RF discharge electrodes.

The principal culprit of the power loss was quenching of the lasing state I* by the copious oxygen atoms in the He/O_2 discharge effluent ($I^* + O \rightarrow I + O$).[12,14] The initial approach to solving this problem was removal of the atoms by NO_2 titration, which allowed a recovery of the $O_2(a)$ concentrations to levels observed without iodine injection. In further work, improved performance was achieved through the addition of NO to the discharge itself. The theoretical rationale for this was to reduce the discharge E/N (through the lower ionization potential of NO) which would allow for a more favorable electron temperature for direct electronic excitation of $O_2(a)$. This approach resulted in a 60% increase in $O_2(a)$ yield which saturated at less than 0.05 mmol/s NO for a 3:16 mmol/s O_2:He flow at 12.5 Torr and 500 W RF.[25] However, that NO flow rate resulted in only a 1% reduction in discharge RF voltage,[14] so the large change in $O_2(a)$ production is not likely to be caused by improved electronic excitation alone. The enhancement of $O_2(a)$ downstream with the addition of NO could be due to a reduction of the deleterious O atom deactivation, or it could be the result of enhanced production due to the recombination of O with the NO_2 formed in the discharge. Whatever the final explanation, the addition of NO is clearly beneficial to ElectricOIL.

Figure 2 shows the significant increase in $O_2(a)$ observed with NO addition for two typical laser operating conditions. These data were taken by translating the diagnostic fiber optics along a quartz flow tube. The increase is larger in the 3:16 O_2:He case, where the oxygen atom yield (without NO) is significantly larger; oxygen atom yield is approximately linear with the ratio of RF power to partial pressure of oxygen.[25] With the enhancement due to NO, the $O_2(a)$ power flux is ~60 W for the 3:16 O_2:He case and ~100 W for the 10:33 O_2:He case. Figure 3 shows the effect of NO on the $O_2(b)$ decay downstream of the

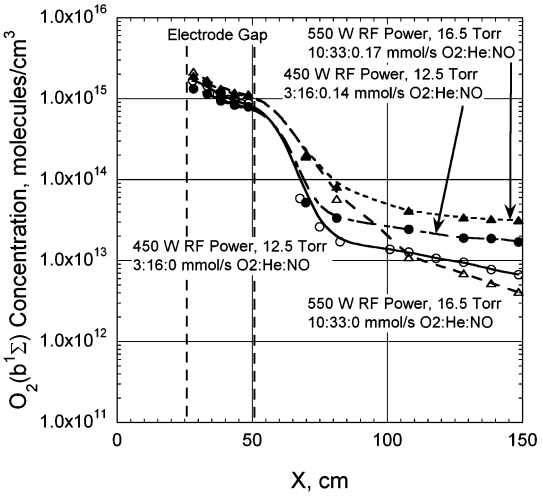

Figure 3. Effect on NO addition on O_2(b) concentration as a function of position and flow conditions.

discharge for the cases from Figure 2. The decay in all cases is rapid but is reduced in the presence of NO, resulting in an order of magnitude increase in O_2(b) at the end of the diagnostic region for the O_2:He = 10:33 mmol/s case and approximately a factor of 3 increase in O_2(b) at the end of the diagnostic region for the O_2:He = 3:16 mmol/s case. This result suggests that the NO flow depletes oxygen atoms which rapidly quench O_2(b). Note that the O_2(a) and O_2(b) concentrations are high at the beginning of the electrode gap, which indicates that a significant amount of power deposition occurs upstream of the physical gap (partially inside the upstream hollow cathode electrode, but the discharge is also visible upstream of the electrode itself). Also note that the temperature (shown later in Figure 7) rises inside the discharge such that the yield of O_2(a) and O_2(b) actually are increasing in the electrode gap (not shown for brevity).

3.2. Depletion of Oxygen Atoms and Ozone with Nitric Oxide. The presence of NO leads to a significant reduction in the oxygen atom flow rate via a recycling process first proposed by Zimmerman et al.,[25] reactions 1 and 2, and supported by modeling predictions with the earlier BLAZE-II code.[15] Oxygen atoms recombine with NO through three-body reactions with O_2 and He to form NO_2, which then further rapidly depletes oxygen atoms by the reaction O + NO_2 → O_2 + NO (see Kaufman).[26] While this latter reaction is exothermic (1.995 eV) and has enough energy to produce both O_2(a) and O_2(b), measurements indicate that the branching ratio to O_2(a) is <5%[13] (also supported by earlier premixed modeling predictions with the BLAZE-II code).[15] Reactions 1a and 1b are published rates for air (applied to oxygen) and argon (applied to helium), respectively. A possible discharge reaction that we believe may be playing an important role in this recycling process is reaction 3; the rate for this reaction is unknown but is believed to be fast [note: reaction 3 is not presently included in the BLAZE-IV modeling]. Reactions 1−3 all remove atomic oxygen and thus reduce the deleterious deactivation of O_2(a) by reaction (4).

$$O + NO + O_2 \rightarrow NO_2 + O_2$$
$$k_{1a} = 4.68 \times 10^{-28} \times T^{-1.5}\ \text{cm}^6/\text{s [ref 27]} \quad (1a)$$

$$O + NO + He \rightarrow NO_2 + He$$
$$k_{1b} = 2.08 \times 10^{-28} \times T^{-1.41}\ \text{cm}^6/\text{s [ref 27]} \quad (1b)$$

$$O + NO_2 \rightarrow O_2 + NO$$
$$k_2 = 6.5 \times 10^{-12} \times e^{(120/T)}\ \text{cm}^3/\text{s [ref 27]} \quad (2)$$

$$NO + O^- \rightarrow NO_2 + e^- \qquad k_3 = \text{unknown (fast)} \quad (3)$$

$$O + O_2(a) + O_2 \rightarrow O + 2O_2$$
$$k_4 = 1 \times 10^{-32}\ \text{cm}^6/\text{s [ref 9]} \quad (4)$$

Considering the power increase in O_2(a) with NO addition and the effects of oxygen atoms on the energy transfer between O_2(a) and iodine atoms, measurement of the oxygen atom density in the presence of NO became necessary. Both actinometry and air afterglow methods were implemented for this measurement. Figure 4 (from actinometry) shows the reduction in oxygen atom flow rate with the addition of NO as a function of RF power. The actinometry data were taken using a 4.5-in.-gap capacitively coupled RF discharge located downstream of the primary discharge. The method is similar to the one applied by Braginskiy et al.[23] The calibration factor was determined via comparison to NO_2 titration and is in good agreement with the factor obtained by modeling the excitation of the Ar* and O* pumping using available cross-section data and a Boltzmann solver for the electron distribution function. The effect of NO on the calibration factor is assumed to be minimal due to the proximity of the energy levels of the initial states for the 777 nm (O*) and 750-nm (Ar*) emissions and the insignificant change in electrical parameters observed for the small NO flow rates used. The initial state for the 750 nm emission Ar($2p_1$) has a threshold of 13.48 eV, while the initial state for the 777 nm emission O($3p^5P$) has a threshold of 10.74 eV. A more significant change in electron energy distribution (characteristic energy) would result in a significant shift in the ratio of O* to Ar*, requiring adjustment of the calibration factor.

Figure 5 shows the effect of NO on the decay of oxygen atoms for 3:16 O_2:He at varied pressure. These results were determined by monitoring the NO_2* emission that results from O + NO recombination at 580 nm with a PMT. The PMT is first calibrated via comparison to NO_2 titration ($I_{PMT} = K$[NO][O], with [O] determined from a NO_2 titration), and the oxygen atom density is obtained by [O] = I_{PMT}/K[NO]. In the cases without NO flowing through the discharge, NO is injected downstream, and a correction is applied to account for O +

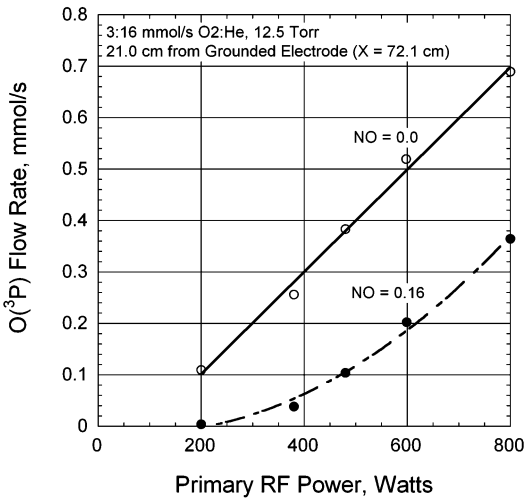

Figure 4. Effect of NO on oxygen atom flow rates determined using Ar actinometry in a 20 W secondary discharge using the 777-nm O* line referenced to the 750-nm Ar* line. The calibration factor is assumed the same for both cases.

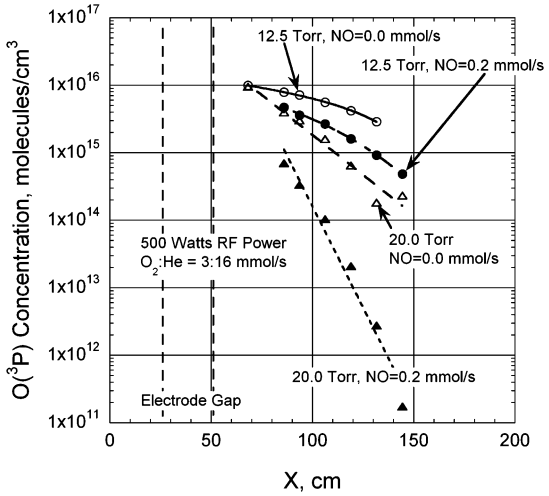

Figure 5. Decay of oxygen atoms downstream of hollow-cathode RF discharge. The oxygen atom concentration is determined by monitoring the NO_2* emission with a calibrated PMT.

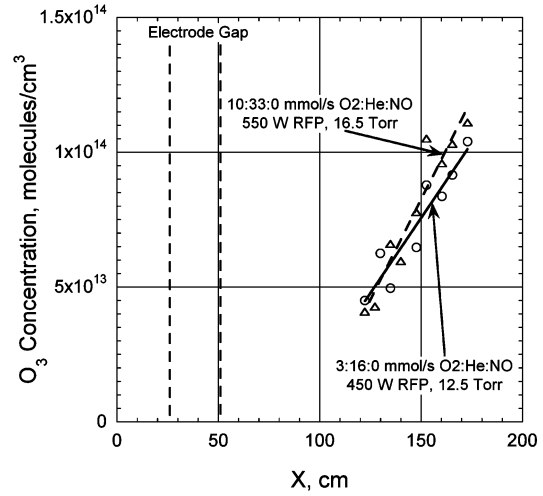

Figure 6. Ozone measurements taken for two different flow conditions. Measurements of ozone with NO in the discharge gas mixture were below the detection limit of the sensitive PSI microabsorbance ozone monitor.

NO recombination such that $[O]_{cor} = [O]_{obs}e^{\alpha t}$, where α is a function of O + NO + M recombination rates and t is the residence time between the injection and the measurement point, assuming average temperatures (and velocities) determined from the O_2(b) spectra at 762 nm. In the cases with NO flowing through the discharge, the NO density along the tube can be determined from the NO input flow rate and total gas density, and the observed [O] is reported. The addition of 0.2 mmol/s of NO to the discharge results in a significant increase in the oxygen atom decay, with the decay also increasing substantially with pressure (between 12.5 and 20 Torr), such that the oxygen atoms are almost completely recombined by the end of the diagnostic region.

Ozone concentration measurements were also taken with the Physical Sciences Inc. microabsorbance ozone monitor,[24] Figure 6. Several interesting effects can be seen from this data. First, for the 3:16 discharge mixture of O_2:He at 12.5 Torr, the measured O_3 increases with distance from the discharge exit going from approximately 4.5×10^{13} cm^{-3} at $X = 120$ cm up to 1.0×10^{14} cm^{-3} at $X = 175$ cm with a discharge power of 450 W; this indicates that the ozone concentration is increasing with distance when there is zero NO flow through the discharge. At 450 W, and at $X = 175$ cm, the O_2 concentration is 5.2×10^{16} cm^{-3} and the O_2(a) concentration is 5.6×10^{15} cm^{-3}; thus, the ozone concentration is only about 0.8% of the O_2(a). Second, for the 10:33 discharge mixture of O_2:He at 16.5 Torr, the measured O_3 was approximately 1.1×10^{14} cm^{-3} at $X = 175$ cm with a discharge power of 550 W; this shows that the ozone concentrations are increased at higher pressures when there is zero NO flow through the discharge, but not dramatically so. Third, and most importantly, when NO is added to the discharge gas mixture, the ozone concentrations were below the detection limit of the instrument for both flow conditions; therefore, the ozone concentration in the presence of NO was $<1 \times 10^{12}$ cm^{-3}, which is a low concentration and would play a minor role in the ElectricOIL kinetics. Note that these results are qualitatively the same as those shown earlier in Palla et al.[28] Gas temperature data for the cases shown in Figures 2 and 3 are shown in Figure 7. The gas temperature is determined from the ratio of two rotational lines in the P-branch of the 762 nm emission of O_2-(b).[5] The uncertainty of this temperature measurement is ±4%.

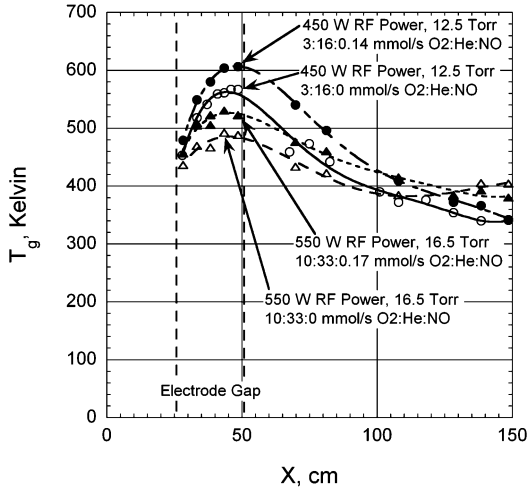

Figure 7. Gas temperature data for cases the shown in Figures 2 and 3.

4. BLAZE-IV And Modeling Results

4.1. BLAZE-IV Discharge Model. In this work a one-dimensional, fluid-dynamic, chemical-kinetic, nonequilibrium plasma-dynamic flow model was developed to investigate the physics critical to the production of O_2(a) in ElectricOIL devices. The model is denoted BLAZE-IV, a new model based partially on BLAZE-II,[15,29,30] the one-dimensional, fluid-dynamic, chemical-kinetic model from which the non-mixing, fluid-dynamic equations used in BLAZE-IV were derived. BLAZE-IV was developed using the C++ programming language to simplify the coding of complex physics by taking advantage of object-oriented programming techniques and appropriate data encapsulation.

BLAZE-IV utilizes the one-dimensional momentum, continuity, energy, and species concentration equations (neutral and charged) and an implicit Newton iteration scheme.[31] The electron-neutral reaction set was compiled from Phelps,[32] Matejcik et al.,[33] Laher and Gilmore,[34] and Cosby,[35] with several unlisted reactions for higher electronic levels estimated to have rates equal to that of the ground state reaction shifted by the energy differences (an approach similar to that taken by Napartovich et al.).[36] An expanded neutral−neutral species chemical kinetic reaction set was derived from the neutral−neutral species and reaction set described by Palla et al.[15] Elastic electron impact momentum transfer reactions have been included for each species, and all critical inelastic electron impact

excitation, ionization, and reattachment processes, in addition to super-elastic processes, have been included in the plasma kinetic reaction set. Chemical kinetic reaction rates are computed from input reaction rate equations, and plasma kinetic reaction rates are computed from input reaction cross sections and electron energy distribution functions derived from the solution of the Boltzmann equation. BLAZE-IV employs a user input power deposition model in which power deposition per volume is specified as a function of axial location via specification of voltage and current.

The BLAZE-IV model solves the classical two-term spherical harmonic expansion of the Boltzmann equation at every integration step to obtain a solution for the nonequilibrium electron energy distribution function using a modified scheme based on the method described by Rockwood.[37] As a result, mean electron energy (electron temperature) may be computed from the calculated distribution function at each integration step rather than solved as a dependent variable. In the method outlined by Rockwood, electron energy is discretized into k cells of fixed width $\Delta\epsilon$ and energy ϵ_k such that the steady state solution for the number of electrons in each energy cell, n_k, may be calculated by using either a forward marching numerical integration scheme or a numerical relaxation technique. Because in the modeled cases uncharged particle densities may be as much as six orders of magnitude greater than electron number density, electron−electron interactions have been excluded. In the BLAZE-IV model, this technique is used to derive a set of k coupled linearized equations that describe the time rates of change in electron number density in each energy cell,

$$\dot{n}_k = C_{kl} n_l \tag{5}$$

where the matrix C_{kl} is non-singular, preventing a direct solution method from deriving the non-trivial steady state solution ($C_{kl}n_l = 0$). However, if we seek as our goal to solve for a normalization of the steady state solution for the electron distribution function in the form $f_k = n_k/n_e$, where total electron number density n_e is unknown, we can make the arbitrary assumption that $n_{k=0}$ is unity and solve accordingly. We then normalize such that all f_k sum to unity, and it is then possible to derive the desired electron energy distribution function to within the normalization constant, n_e. Using this technique, knowledge of the absolute total electron number density (the normalization constant, n_e) is not preserved through the solution method and therefore must be obtained using other means. BLAZE-IV derives the necessary total electron number density by calculating the elastic and inelastic electron-particle collision frequencies using input momentum transfer cross sections for each species i (σ_i), input inelastic electron/heavy particle collision cross sections for species i and inelastic reaction j (σ_{ij}), the normalized electron energy distribution function (f_k), and absolute heavy particle species concentrations (n_i),

$$\bar{\nu}_i \equiv n_i \int_0^\infty f(\epsilon)\, \sigma_i(\epsilon)\, \upsilon(\epsilon)\, \mathrm{d}\epsilon = n_i \sum_k f_k \sigma_i(\epsilon_k)\, \upsilon(\epsilon_k) \tag{6}$$

$$\bar{\nu}_j \equiv n_i \int_0^\infty f(\epsilon)\, \sigma_{ij}(\epsilon)\, \upsilon(\epsilon)\, \mathrm{d}\epsilon = n_i \sum_k f_k \sigma_{ij}(\epsilon_k)\, \upsilon(\epsilon_k) \tag{7}$$

Using the calculated normalized elastic and inelastic collision frequencies, we may compute the power deposition per electron using a calculated value for the mean energy exchanged in an elastic collision and specified values for inelastic reaction energies, $\Delta\epsilon_j$,

$$\bar{P} \equiv \sum_i \frac{3}{2} \bar{\nu}_i \left(\frac{2m_e}{M_i}\right) k_B (T_e - T_g) + \sum_j \bar{\nu}_j \Delta\epsilon_j \tag{8}$$

It is then possible to compute the total electron number density and absolute electron impact reaction rates by dividing the specified power deposition rate by the calculated value for power deposited per electron. This method enforces consistency given a specified power deposition model. Note that although T_e and n_e are calculated independently of an electron energy equation, the effect of the net change in total energy stored in electrons may still be included in the energy equation by including a pre-evaluated term of the form $(\Delta T_e \Delta n_e)/\Delta x$. As a verification of the above scheme, the calculated energy distribution functions from BLAZE-IV for electrons in helium, Figure 8, reproduced calculations in refs 38−40. In addition, experimental values for electron drift velocity and electron temperature as function of the ratio of the electric field to gas number density were also reproduced accurately, Figure 9.

4.2. Peak Yield and Optimum E/N Calculations. Using the nonequilibrium plasmadynamics capability of the BLAZE-IV model, physics critical to the improvement of ElectricOIL devices have been studied. For the purposes of this study $O_2(a^1\Delta)$ yield is defined as the ratio of the $O_2(a^1\Delta)$ state to all states of the O_2 molecule.

$$\text{yield} \equiv \frac{[O_2(a^1\Delta)]}{[O_2(^3X)] + [O_2(a^1\Delta)] + [O_2(b^1\Sigma)] + {}^3/_2[O_3] + {}^1/_2[O]} \tag{9}$$

Calculations indicate that in a high-yield discharge, the equilibrium yield value is dominated by the equilibrium achieved between the inelastic electron impact excitation of $O_2(^3X)$ to $O_2(a^1\Delta)$ and its super-elastic reverse. Calculations indicate that this yield equilibrium may exhibit dependence on a range of discharge parameters.

To illustrate this effect, calculations were performed for a O_2:He:NO = 3:16:0.15 mmol/s discharge at 12.5 Torr. All ElectricOIL calculations utilized a discretization of the electron energy used in the solution of the Boltzmann equation into 100 cells with a constant energy cell width over the range 0−25 eV. As the yield equilibrium in this case is, to first order, dominated by an equilibrium between electron impact events, total electron number density may be factored out, therefore making the resulting calculated yield equilibrium independent of power deposition, assuming E/N may be held fixed, independent of applied power. It should be noted, however, that applied power may strongly impact discharge gas temperature and electric field strength (in addition to other flow parameters) and therefore may indirectly influence the electron energy distribution function and any resulting equilibrium achieved between competing electron impact events. The $O_2(a^1\Delta)$ yield equilibrium in this case is characterized by the simplified net fraction of power deposited into $O_2(a^1\Delta)$. The simplified net fraction of power deposited into $O_2(a^1\Delta)$ is defined as the ratio of net power deposited into $O_2(a^1\Delta)$ [power deposited by electron impact excitation of $O_2(^3X)$ to $O_2(a^1\Delta)$ less power lost via the super-elastic reverse] to the net power deposited into the flow via all elastic and inelastic processes. When the simplified net fraction of power deposited into $O_2(a^1\Delta)$ is plotted versus the ratio of the electric field to gas number density for discharge start-up conditions (initially zero yield), the positive peak of the resulting curve may be considered the optimum E/N value for the net positive production of $O_2(a^1\Delta)$ in the modeled

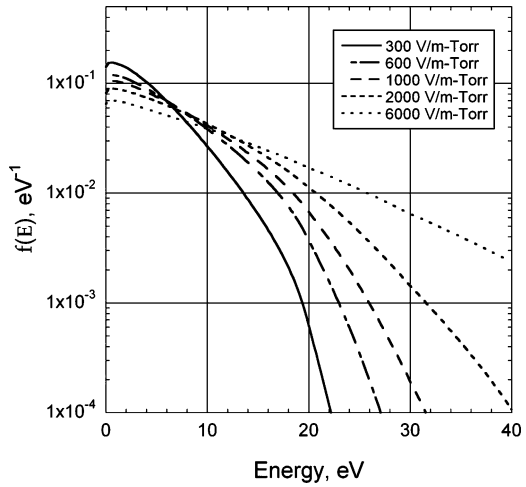

Figure 8. BLAZE-IV calculated electron energy distribution functions for electrons in helium as a function of the ratio of the electric field to the gas pressure. The computed results match data from Cherington,[38] found originally in Smit,[39] and Reder and Brown[40]

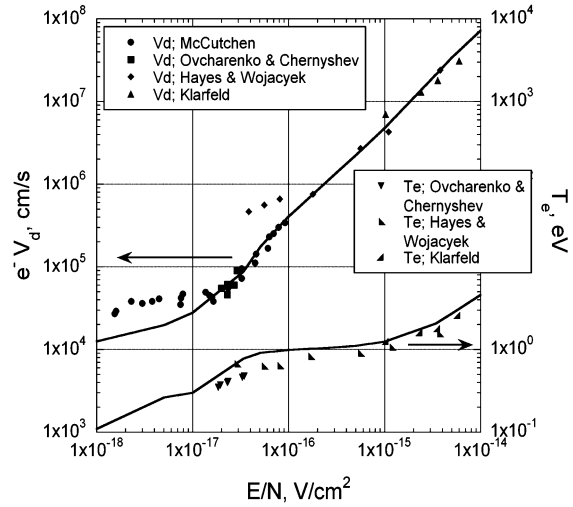

Figure 9. BLAZE-IV calculated electron drift velocity and electron temperature for electrons in helium. Reproduction of data from Klarfeld,[41] McCutchen,[42] Ovcharenko and Chernyshev,[43] and Hayes and Wojacyek[44]

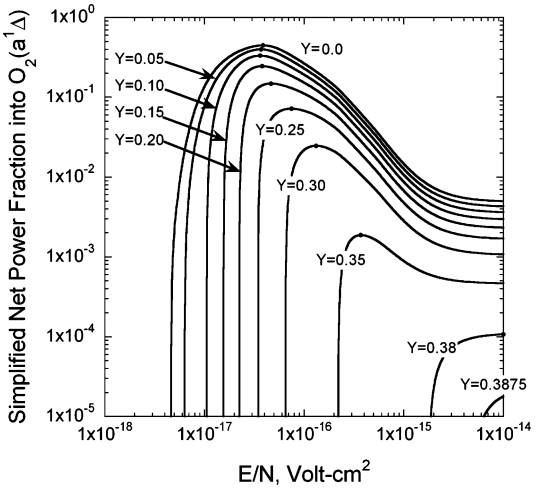

Figure 10. BLAZE-IV calculated ratio of simplified net power deposited into $O_2(a^1\Delta)$ (power deposited by electron impact excitation of $O_2(^3X)$ less power lost via super-elastic collisions) to the net power deposited into the flow via all elastic and inelastic processes. Also highlighted are curve peaks which correspond to the approximate optimum *E*/*N* value for each simulated yield.

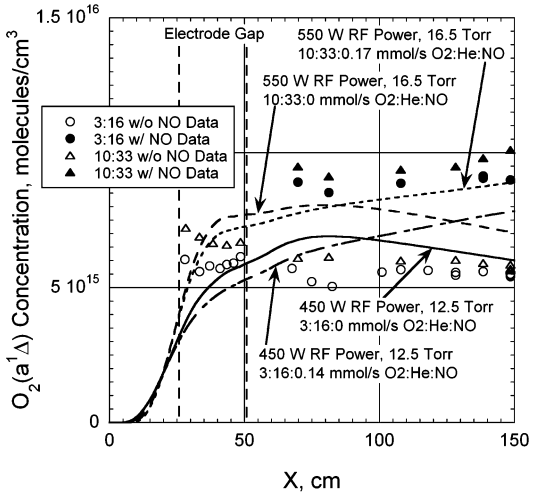

Figure 11. BLAZE-IV calculated $O_2(a^1\Delta)$ concentration versus axial location, discharge flow rates, and pressure compared with data. Comparison data are also presented above in Figure 2.

electric discharge. Calculations indicate that for this discharge start-up condition ($Y = 0.0$) the optimum *E*/*N* value for the production of $O_2(a^1\Delta)$ for the modeled discharge is approximately 3.9 Td (1 Townsend (Td) $= 1 \times 10^{-17}$ V cm^2), Figure 10.

However, when the same study is performed for an operating discharge (nonzero yield, $Y > 0$, and concentrations of other states typical to an operating discharge) the location of the peak shifts to higher E/N values. For example, with a O_2:He:NO = 3:16:0.15 mmol/s gas mixture at 12.5 Torr having an $O_2(a^1\Delta)$ yield of 0%, the peak fractional power deposition is 0.445 at 3.9 Td for these flow conditions, whereas at a yield of 0.3 the peak fractional power deposition is approximately 0.025 at 13.2 Td. Therefore, the above calculations were performed for a range of $O_2(a^1\Delta)$ yields from 0.0 to 0.3875. It was found that for yields above approximately 0.3875, at the above discharge conditions, the power deposition curves approached zero or below, indicating that for these conditions the maximum achievable yield is near 0.3875. This value is close to the achievable yield limit of 0.4 that may be predicted analytically based on an equilibrium energy distribution and the statistical weights of 2 and 3 that are used for the states $O_2(^3X)$ and $O_2(a^1\Delta)$ in the calculation of the collision cross section for the super-elastic de-excitation of $O_2(a^1\Delta)$ to $O_2(^3X)$. In addition, the calculations indicate that the optimum operating *E*/*N* for production of $O_2(a^1\Delta)$ remains generally stable between 3.9 and 7.5 Td for equilibrium yields in the range of 0.0 to 0.25, before shifting to higher values. This indicates that as a discharge stabilizes at an operating yield greater that zero, the optimum operating *E*/*N* may not be constant for certain operating conditions. It should be noted, however, that even for the described discharge, the optimum yield may likely be tuned to higher values using other means such as the attenuation of temperature effects and other possibly detrimental conditions. Furthermore, discharge produced $O_2(b^1\Sigma)$ can be converted to $O_2(a^1\Delta)$ in the post-discharge region, and it may be possible to catalytically convert O atoms into $O_2(a^1\Delta)$, thereby further increasing the $O_2(a^1\Delta)$ yield.

4.3. Singlet Oxygen, Atomic Oxygen, and Ozone Calculations. To test the capabilities of the BLAZE-IV model and analyze recent data, singlet oxygen (delta and sigma), atomic oxygen, and ozone concentrations were modeled as a function of discharge flow rates and pressure. Figures 11−17 show BLAZE-IV calculations compared with data (also presented

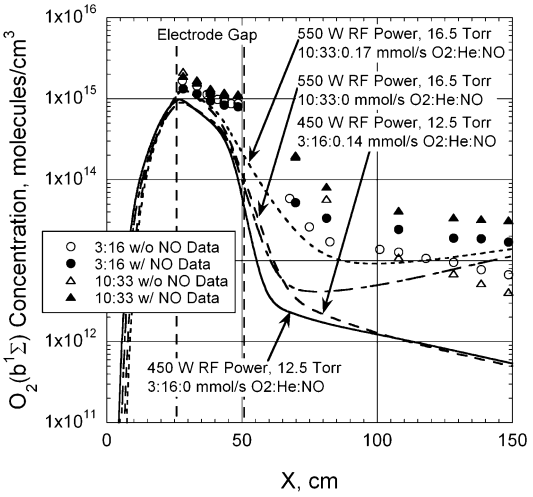

Figure 12. BLAZE-IV calculated $O_2(b^1\Sigma)$ concentration versus axial location, discharge flow rates, and pressure compared with data. Comparison data are also presented above in Figure 3.

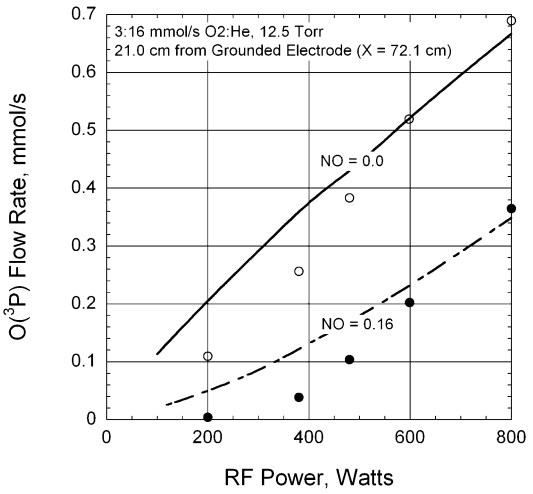

Figure 13. BLAZE-IV calculated $O(^3P)$ flow rate versus RF discharge power with and without NO compared with data. Comparison data are also presented above in Figure 4.

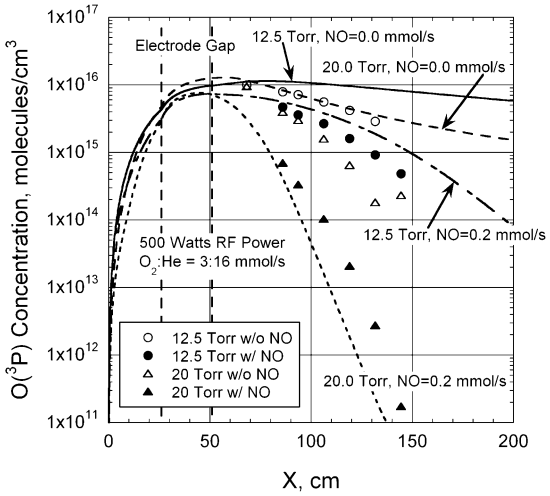

Figure 14. BLAZE-IV calculated $O(^3P)$ concentration vs axial location and discharge pressure, with and without NO with a discharge power of 500 W compared with the data. Comparison data are also presented above in Figure 5.

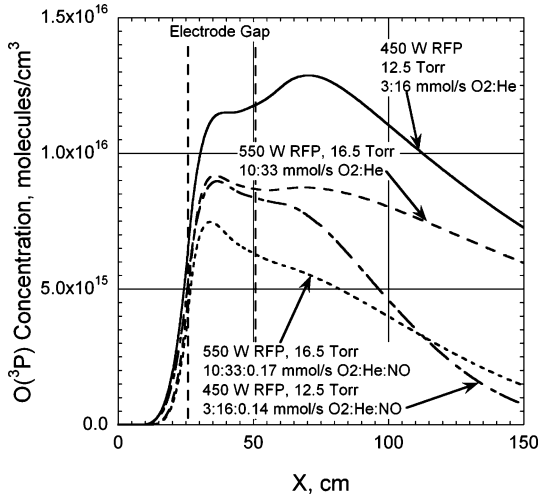

Figure 15. BLAZE-IV calculated O concentration versus axial location, discharge flow rates, and pressure with and without NO.

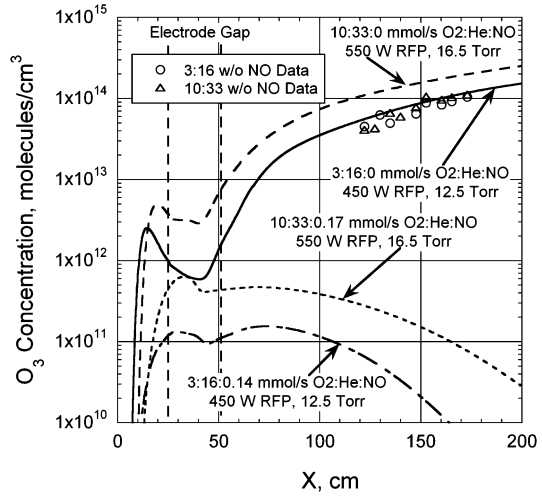

Figure 16. BLAZE-IV calculated O_3 concentration versus axial location, discharge flow rates, and pressure with and without NO compared with data. Comparison data are also presented above in Figure 6.

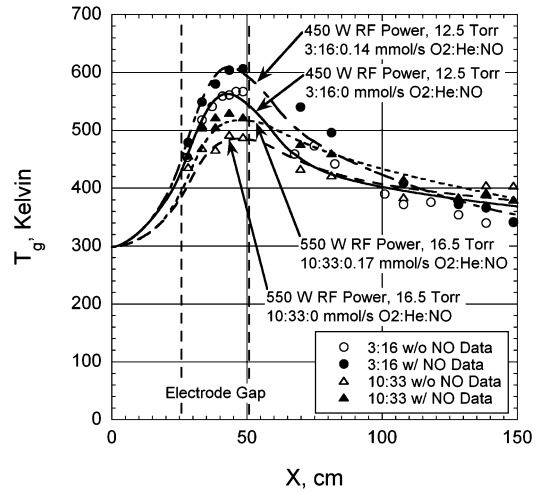

Figure 17. BLAZE-IV calculated gas temperature versus axial location, discharge flow rates, and pressure with and without NO compared with data. Comparison data are also presented above in Figure 7.

above in Figures 2−7). The overall agreement is reasonable for this one-dimensional model, and all of the important trends are being modeled reasonably well, except as noted below regarding the $O_2(a)$ concentrations. In Figure 11, the reactions that are primarily responsible for the deviation between the cases with and without NO in the gas mixture are reactions 1 and 2

above that remove O atoms and prevent the loss of yield via reaction 4. The removal of O atoms also reduces the loss of $O_2(b)$ via the reaction $O + O_2(b) \rightarrow O + O_2(a)$, having a rate of 7.2×10^{-14} cm^3/s.[27] Note that the comparison data (also shown in Figure 2) near the discharge exit have a larger difference in $O_2(a)$ concentration between the with and the without NO cases than the model shows in Figure 11; this suggests that there is still some important process that is missing in the modeling, perhaps reaction 3 or perhaps reaction 2 has a branching fraction to $O_2(a)$ greater than 5% in the elevated temperature conditions of the discharge region.

Many of the quantitative results shown in Figures 11−17 are also in reasonable agreement with the data. Figure 11 shows modeled concentrations of $O_2(a)$ within about ±20% of the data. Figure 12 shows reasonable qualitative agreement with the $O_2(b)$ data (also shown in Figure 3), but the predicted decay is faster than the data indicate. Figure 13 shows reasonable agreement between BLAZE-IV and the O atom data (also presented in Figure 4) as a function of RF discharge power relatively near (21 cm downstream) the discharge exit electrode. Figure 14 shows that the model under-predicts the decay of O atoms with zero NO in the gas mixture. It is unknown at present why there are some deviations from data, but it could be representative of the fact that (i) surface reactions are not yet modeled in BLAZE-IV and (ii) the measured data are in a nonuniform flow field (similar to fully developed pipe flow) because of boundary layers that build up on the walls of the flow tubes, whereas the BLAZE-IV model is one-dimensional. The fact that the model over-predicts the $O_2(b)$ decay, Figure 12, is consistent with the under-prediction of O atom loss, Figure 14; that is, higher O atom concentration leads to a higher decay rate of $O_2(b)$. Thus, whatever mechanism improves agreement with the atomic oxygen concentration data (possibly the inclusion of wall recombination) may also result in an improvement in the $O_2(b)$ predictions.

Atomic oxygen concentration was also modeled as a function of axial location for discharge flow rates of O_2:He = 3:16 mmol/s at 12.5 Torr and O_2:He = 10:33 mmol/s at 16.5 Torr both with and without titrant flow rates of NO = 0.14 mmol/s and 0.17 mmol/s, respectively, Figure 15. The presence of this small amount of NO shows the dramatic effect of reducing the atomic oxygen concentration. This is helpful in two major ways:

1. The effect of the critical $I^* + O(^3P) \rightarrow I + O(^3P)$ quenching reaction (discussed at length by Carroll et al.,[11] Rawlins et al.,[16] and Azyazov et al.[12]) is significantly reduced.

2. The effect of the $O_2(a^1\Delta) + O_2(^3X) + O(^3P) \rightarrow 2\ O_2(^3X) + O(^3P)$ is also significantly reduced.

Predictions of the ozone concentration as compared to data are presented in Figure 16. BLAZE-IV is in good quantitative agreement with the measurements for the O_2:He = 3:16 mmol/s case with a pressure of 12.5 Torr but is under-predicting the O_2:He = 10:33 mmol/s case with a pressure of 16.5 Torr. Perhaps most importantly, the model shows the dramatic drop in ozone when NO is present in the discharge gas mixture, Figure 16, in agreement with the measurements. The result that the O_3 concentration drops significantly with the addition of NO is consistent with modeling by Babaeva et al.[45] Gas temperature data for the cases described in Figures 2, 3, and 7 were well modeled, Figure 17.

5. Summary

In the ElectricOIL system the discharge production of atomic oxygen, ozone, and other excited species adds levels of complexity to the kinetics which are not encountered in a classic purely chemical $O_2(a^1\Delta)$ generation system. To study these phenomena in greater detail, advanced diagnostics were employed to measure the $O_2(a^1\Delta)$, $O_2(b^1\Sigma)$, O_3, and O atom concentrations as a function of flow distance, gas mixture, pressure, and RF discharge power. An advanced model BLAZE-IV has been introduced to study the energy-transfer laser system dynamics and kinetics in the discharge and post-discharge. Levels of singlet oxygen, oxygen atoms, and ozone are measured experimentally and compared with calculations. The new BLAZE-IV model is in reasonable agreement with O_3, O atom, and gas temperature measurements but is under-predicting the increase observed in $O_2(a^1\Delta)$ concentrations in with NO present in the discharge and under-predicting the $O_2(b^1\Sigma)$ concentrations. A key conclusion is that the removal of oxygen atoms by NO and NO_2 species leads to a significant increase in $O_2(a^1\Delta)$ concentrations downstream of the discharge in part via a recycling process of the NO and NO_2 molecules, but there still appears to be some important missing discharge kinetics related to NO and/or NO_2. Further, the removal of oxygen atoms via the use of NO in the discharge gas mixture dramatically inhibits the production of ozone in the downstream kinetics. Note that while O_3 concentrations with NO in the discharge mixture are low at these pressures <20 Torr, it is possible that O_3 may still be significant at higher pressures of >50 Torr when NO is present in the gas mixture. Modeling of the experimental data would likely be improved by the inclusion of wall surface reactions and with the use of a higher dimensional model.

Acknowledgment. This work was supported by the Missile Defense Agency (MDA) through the U.S. Army Space and Missile Defense Command (USA SMDC), the Air Force Office of Scientific Research (AFOSR), the Joint Technology Office (JTO), the Air Force Research Laboratory (AFRL) Directed Energy Directorate, and by CU Aerospace internal research and development funds. The authors acknowledge the contributions of T. Madden and D.A. Hostutler (AFRL); G. Hager (University of New Mexico); W.T. Rawlins, S. Davis, and S. Lee (Physical Sciences Inc.); M. Kushner (Iowa State University); M. Heaven and K. Morokuma (Emory University); G. Perram (Air Force Institute of Technology); M. Berman (AFOSR); J. Mulroy and J. Kotora (MDA); B. Otey (USA/SMDC); Lt. Col. W. Fink (JTO); A. Ionin (P.N. Lebedev Physics Institute); and T. Rakhimova and Yu. Mankelevich (Lomonosov Moscow State University). The authors thank D. King, J. Laystrom, and G. Benavides for their technical assistance.

References and Notes

(1) McDermott, W.; Pchelkin, N.; Benard, D.; Bousek, R. *Appl. Phys. Lett.* **1978**, *32* (8), 469.

(2) Zalesskii, V. Yu. *Zh. Eksp. Teor. Fiz.* **1974**, *67*, 30 [*Sov. Phys. JETP* **1975**, *40* (1), 14].

(3) Fournier, G.; Bonnet, J.; Pigache, D. *J. Physique* **1981**, *41* (Colloque C9), 449.

(4) Carroll, D. L.; Verdeyen, J. T.; King, D. M.; Woodard, B. S.; Skorski, L. W.; Zimmerman, J. W.; Solomon, W. C. *IEEE J. Quantum Electron.* **2003**, *39* (9), 1150.

(5) Carroll, D. L.; Verdeyen, J. T.; King, D. M.; Woodard, B. S.; Zimmerman, J. W.; Skorski, L. W.; Solomon, W. C., Recent Experimental Measurements of the ElectriCOIL System. Presented at 34th AIAA Plasmadynamics and Lasers Conference, Orlando, FL, June 23−26, 2003; AIAA Paper 2003-4029; http://www.aiaa.org (accessed December 2006).

(6) Schmiedberger, J.; Hirahara, S.; Ichinoche, Y.; Suzuki, M.; Masuda, W.; Kihara, Y.; Yoshitani, E.; Fujii, H. *Proc. SPIE-Int. Soc. Opt. Eng.* **2001**, *4184*, 32.

(7) Hill, A. E. In *Proceedings of the International Conference on Lasers 2000*; Corcoran, V., Corcoran, T., Eds.; STS Press: McClean, VA, 2001; p 249.

(8) Ionin, A. A.; Kochetov, I. V.; Napartovich, A. P.; Yuryshev, N. N. Physics and engineering of singlet delta oxygen production in low-temperature plasma. *J. Phys. D: Appl. Phys.* **2007**, *40*, R25.

(9) Rakhimova, T. V.; Kovalev, A. S.; Rakhimov, A. T.; Klopovsky, K. S.; Lopaev, D. V.; Mankelevich, Y. A.; Proshina, O. V.; Braginsky, O. V.; Vasilieva, A. N. Radio-Frequency Plasma Generation of Singlet ($a^1\Delta_g$) Oxygen in O_2 and O_2:Ar (He) Mixtures. Presented at 34th AIAA Plasmadynamics and Lasers Conference, Orlando, FL, June 23−26, 2003; AIAA Paper 2003-4306; http://www.aiaa.org (accessed December 2006).

(10) Carroll, D. L.; Verdeyen, J. T.; King, D. M.; Zimmerman, J. W.; Laystrom, J. K.; Woodard, B. S.; Richardson, N.; Kittell, K.; Kushner, M. J.; Solomon, W. C. Measurement of positive gain on the 1315 nm transition of atomic iodine pumped by $O_2(a^1\Delta)$ produced in an electric discharge. *Appl. Phys. Lett.* **2004**, *85* (8), 1320−1322.

(11) Carroll, D. L.; Verdeyen, J. T.; King, D. M.; Zimmerman, J. W.; Laystrom, J. K.; Woodard, B. S.; Benavides, G. F.; Kittell, K.; Stafford, D. S.; Kushner, M. J.; Solomon, W. C. Continuous-wave laser oscillation on the 1315 nm transition of atomic iodine pumped by $O_2(a^1\Delta)$ produced in an electric discharge. *Appl. Phys. Lett.* **2005**, *86*, 111104.

(12) Azyazov, V. N.; Antonov, I.; Ruffner, S.; Heaven, M. C. Quenching of $I(^2P_{1/2})$ by O_3 and $O(^3P)$. *Proc. SPIE-Int. Soc. Opt. Eng.* **2006**, *6101*, 61011Y.

(13) Azyazov, V. N.; Antonov, I. O.; Kabir, H.; Heaven, M. C. Chemical kinetics of discharge driven oxygen-iodine lasers. Presented at GCL-HPL 2006 Conference, Gmunden, Austria, September 4−8, 2006.

(14) Carroll, D. L.; Verdeyen, J. T.; King, D. M.; Zimmerman, J. W.; Laystrom, J. K.; Woodard, B. S.; Benavides, G. F.; Kittell, K.; Solomon, W. C. Path to the measurement of positive gain on the 1315 nm transition of atomic iodine pumped by $O_2(a^1\Delta)$ produced in an electric discharge. *IEEE J. Quantum Electron.* **2005**, *41* (2), 213−223.

(15) Palla, A. D.; Carroll, D. L.; Verdeyen, J. T.; Solomon, W. C. Mixing Effects in Post-Discharge Modeling of ElectricOIL Experiments. *J. Appl. Phys*. **2006**, *100*, 023117.

(16) Rawlins, W. T.; Lee, S.; Kessler, W. J.; Davis, S. J. *Appl. Phys. Lett.* **2005**, *86*, 051105-1-3.

(17) Verdeyen, J. T.; Carroll, D. L.; King, D. M.; Laystrom, J. K.; Benavides, G. F.; Zimmerman, J. W.; Woodard, B. S.; Solomon, W. C. Continuous-wave laser oscillation in subsonic flow on the 1315 nm atomic iodine transition pumped by electric discharge produced $O_2(a^1\Delta)$. *Appl. Phys. Lett.* **2006**, *89*, 101115.

(18) Hicks, A.; Utkin, Y.; Lempert, W. R.; Rich, J. W.; Adamovich, I. V. Presented at GCL-HPL 2006 Conference, Gmunden, Austria, September 4−8, 2006.

(19) Stafford, D. S.; Kushner, M. J. $O_2(^1\Delta)$ production in flowing He/O2 plasmas. I. Axial transport and pulsed power formats, *J. Appl. Phys*. **2006**, *98*, 073303.

(20) Babaeva, N. Y.; Arakoni, R. A.; Kushner, M. J. Production of $O_2(^1\Delta)$ in flowing plasmas using spiker-sustainer excitation. *J. Appl. Phys*. **2006**, *99*, 113306.

(21) Rakhimova, T. V.; Kovalev, A. S.; Lopaev, D. V.; Proshina, O. V.; Mankelevich, Yu. A.; Kolobyanin, Yu. V.; Braginsky, O. V.; Klopovsky, K. S.; Popov, N. A.; Rakhimov, A. T.; Vasilieva, A. N. Singlet oxygen generator operating at high oxygen pressure. Presented at 37th AIAA Plasmadynamics and Lasers Conference, San Francisco, CA, June 5−8; AIAA Paper 2006-3762; http://www.aiaa.org (accessed December 2006).

(22) Proshina, O. V.; Rakhimova, T. V.; Braginsky, O. V.; Kovalev, A. S.; Lopaev, D. V.; Mankelevich, Yu. A.; Rakhimov, A. T.; Vasilieva, A. N. Discharge singlet oxygen generator for oxygen-iodine laser: II. Two-dimensional modelling of flow oxygen rf plasma at 13.56 and 81 MHz power frequency. *J. Phys. D* **2006**, *39*, 5191.

(23) Braginskiy, O.; Vasilieva, A.; Klopovskiy, K.; Kovalev, A.; Lopaev, D.; Proshina, O.; Rakhimova, T.; Rakhimov, A. Singlet oxygen generation in O2 flow excited by RF discharge: I. Homogeneous discharge mode: α-mode. *J. Phys. D: Appl. Phys*. **2005**, *38*, 3609−3625.

(24) Rawlins, W. T. PSI Microabsorbance Monitors for Iodine and Ozone: System Description. PSI technical report PSI-2908/TR-2114; Physical Sciences Inc.: Andover, MA, 2006.

(25) Zimmerman, J. W.; King, D. M.; Palla, A. D.; Verdeyen, J. T.; Carroll, D. L.; Laystrom, J. K.; Benavides, G. F.; Woodard, B. S.; Solomon, W. C.; Rawlins, W. T.; Davis, S. J.; Heaven, M. C. Important kinetic effects in the hybrid ElectricOIL system. *Proc. SPIE-Int. Soc. Opt. Eng.* **2006**, *6261*, 62611R.

(26) Kaufman, F. *Proc. R. Soc. London, Ser. A* **1958**, *247*, 123.

(27) Atkinson, R.; Baulch, D.; Cox, R.; Hampson, R., Jr.; Kerr, J.; Rossi, M.; Troe, J. *J. Phys. Chem. Ref. Data* **1997**, *26*, 3.

(28) Palla, A. D.; Zimmerman, J. W.; Woodard, B. S.; Carroll, D. L.; Verdeyen, J. T.; Lim, T. C.; Rawlins, W. T.; Lee, S.; Davis, S. J.; Solomon, W. C. ElectricOIL discharge and post-discharge experiments and modeling. *Proc. SPIE-Int. Soc. Opt. Eng.* **2007**, *6454*, 645419.

(29) Sentman, L. H.; Subbiah, M.; Zelazny, S. *Blaze II: a chemical laser simulation computer program*; Technical Report H-CR-77-8; Bell Aerospace Textron: Buffalo, NY, 1977.

(30) Carroll, D. L. *AIAA J.* **1995**, *33* (8), 1454−1462.

(31) Byrne, G. D.; Hindmarsh, A. C. Stiff ODE Solvers: A Review of Current and Coming Attractions. *J. Comput. Phys.* **1987**, *70*, 1−62.

(32) Phelps, A. V. Compilation of Electron Cross Sections. Unpublished text available via A. V. Phelps website: ftp://jila.colorado.edu/collision_data/electronneutral/electron.txt (latest update 2005).

(33) Matejcik, S.; Kiendler, A.; Cicman, P.; Skalny, J.; Stampfli, P.; Illenberger, E.; Chu, Y.; Stamatovic, A.; Mark, T. D. *Plasma Sources Sci. Technol.* **1997**, *6*, 140−146.

(34) Laher, R. R.; Gilmore, F. R. Updated Excitation and Ionization Cross Sections for Electron Impact on Atomic Oxygen. *J. Phys. Chem. Ref. Data* **1990**, *19*, 277.

(35) Cosby, P. C. Electron-impact dissociation of oxygen. *J. Chem. Phys*. **1993**, *98*, 9560−9569.

(36) Napartovich, A. P.; Deryugin, A. A.; Kochetov, I. V. *J. Phys. D: Appl. Phys*. **2001**, *34*, 1827−1833.

(37) Rockwood, S. D. Elastic and Inelastic Cross Sections for Electron-Hg Scattering from Hg Transport Data. *Phys. Rev. A* **1975**, *8* (5), 2348.

(38) Cherington, B. E. *Gaseous Electronics and Gas Lasers*; Pergamon Press: New York, 1979; p 71.

(39) Smit, J. A. Berechnung der Geschwindigkeitsverteilung der elektronen bei Gasentladungen in Helium. *Physica* **1936**, *3*, 543−560.

(40) Reder, F. H.; Brown, S. C. Energy Distribution function of Electrons in Pure Helium. *Phys. Rev.* **1954**, *95*, 885−889.

(41) Klarfeld, B. *Tech. Phys.* **1938**, *5*, 913.

(42) McCutchen, C. W. *Phys. Rev.* **1958**, *112*, 1848.

(43) Ovcharenko, V. A.; Chernyshev, S. M. *Teplofiz. Vys. Temp*. **1970**, *8*, 716.

(44) Hayes, E.; Wojacyek, K. *Beitr. Plasmaphys.* **1963**, *3*, 74.

(45) Babaeva, N.; Arakoni, R.; Kushner, M. Strategies for higher yields of $O_2(^1\Delta)$ at higher pressures for electrically excited chemical oxygen-iodine lasers. Presented at the Electric Oxygen-Iodine Laser Workshop, Albuquerque, NM, May, 2006.